J|A|C|S
ARTICLES
Published on Web 12/19/2006

Proton Shuttles and Phosphatase Activity in Soluble Epoxide Hydrolase

Marco De Vivo,* Bernd Ensing, Matteo Dal Peraro, German A. Gomez, David W. Christianson, and Michael L. Klein

Contribution from the Department of Chemistry, University of Pennsylvania, 231 South 34th Street, Philadelphia, Pennsylvania 19104-6323

Received August 24, 2006; E-mail: mdevivo@cmm.upenn.edu

Abstract: Recently, a novel metal Mg^{2+}-dependent phosphatase activity has been discovered in the N-terminal domain of the soluble epoxide hydrolase (sEH), opening a new branch of fatty acid metabolism and providing an additional site for drug targeting. Importantly, the sEH N-terminal fold belongs to the haloacid dehalogenase (HAD) superfamily, which comprises a vast majority of phosphotransferases. Herein, we present the results of a computational study of the sEH phosphatase activity, which includes classical molecular dynamics (MD) simulations and mixed quantum mechanical/molecular mechanics (QM/MM) calculations. On the basis of experimental results, a two-step mechanism has been proposed and herein investigated: (1) phosphoenzyme intermediate formation and (2) phosphoenzyme intermediate hydrolysis. Building on our earlier work, we now provide a detailed description of the reaction mechanism for the whole catalytic cycle along with its free energy profile. The present computations suggest metaphosphate-like transition states for these phosphoryl transfers. They also reveal that the enzyme promotes water deprotonation and facilitates shuttling of protons via a metal−ligand connecting water bridge (WB). These WB-mediated proton shuttles are crucial for the activation of the solvent nucleophile and for the stabilization of the leaving group. Moreover, due to the conservation of structural features in the N-terminal catalytic site of sEH and other members of the HAD superfamily, we suggest a generalization of our findings to these other metal-dependent phosphatases.

Introduction

Phosphatases are enzymes that catalyze the hydrolysis of phosphate esters from a variety of phosphorylated substrates, ranging from specific Thr/Ser residues of proteins to nonprotein substrates such as phospholipids. Phosphate ester hydrolysis is a hallmark of biochemical processes crucial in signal transduction pathways and cell cycle regulation.[1−6] The mechanism of enzymatic phosphoryl transfers has been extensively studied in many different enzymes, such as GTPases[7−10] and protein kinases.[11,12] An extreme increase of the reaction rate by as much as $\sim 10^{21}$ and different possible pathways (dissociative, associative, or concerted) as induced by the specific chemical environment have been reported.[13,14]

In this study, we focus on a recently discovered phosphatase activity exhibited by the dual domain protein, human soluble epoxide hydrolase[15,16] (sEH; Figure 1). The initially observed catalytic activity of sEH, namely the hydrolysis of epoxy fatty acids, occurs in the large C-terminal domain. The mechanism of the epoxide hydrolysis reaction is now well understood,[15,17] and the inhibition of sEH is a potential therapeutic strategy for the treatment of hypertension, cancer progression, and acute inflammation conditions.[18−20] The novel metal Mg^{2+}-dependent phosphatase activity of sEH, on the other hand, has been recently discovered in the smaller N-terminal domain,[21,22] and as of yet, very little is known about its biological function. Crystal structures of human sEH provided evidence for bifunctional catalysis, showing a product complex with HPO_4^{2-} and a hexacoordinated Mg^{2+} ion bound in the active site of the

(1) Morrison, J. F.; Heyde, E. *Annu. Rev. Biochem.* **1972**, *41*, 29−54.
(2) Knowles, J. R. *Annu. Rev. Biochem.* **1980**, *49*, 877−919.
(3) Jackson, M. D.; Denu, J. M. *Chem. Rev.* **2001**, *101*, 2313−2340.
(4) Kennelly, P. J. *Chem. Rev.* **2001**, *101*, 2291−2312.
(5) Johnson, L. N.; Lewis, R. J. *Chem. Rev.* **2001**, *101*, 2209−2242.
(6) Dzeja, P. P.; Terzic, A. *J. Exp. Biol.* **2003**, *206*, 2039−2047.
(7) Wittinghofer, A. *Trends Biochem. Sci.* **2006**, *31*, 20−23.
(8) Glennon, T. M.; Villa, J.; Warshel, A. *Biochemistry* **2000**, *39*, 9641−9651.
(9) Du, X. L.; Black, G. E.; Lecchi, P.; Abramson, F. P.; Sprang, S. R. *Proc. Natl. Acad. Sci. U.S.A.* **2004**, *101*, 8858−8863.
(10) Li, G. P.; Zhang, X. J. C. *J. Mol. Biol.* **2004**, *340*, 921−932.
(11) Diaz, N.; Field, M. J. *J. Am. Chem. Soc.* **2004**, *126*, 529−542.
(12) Cheng, Y. H.; Zhang, Y. K.; McCammon, J. A. *J. Am. Chem. Soc.* **2005**, *127*, 1553−1562.
(13) Cleland, W. W.; Hengge, A. C. *Chem. Rev.* **2006**, *106*, 3252−3278.
(14) Allen, K. N.; Dunaway-Mariano, D. *Trends Biochem. Sci.* **2004**, *29*, 495−503.
(15) Morisseau, C.; Hammock, B. D. *Annu. Rev. Pharmacol. Toxicol.* **2005**, *45*, 311−333.
(16) Newman, J. W.; Morisseau, C.; Hammock, B. D. *Prog. Lipid Res.* **2005**, *44*, 1−51.
(17) Schiott, B.; Bruice, T. C. *J. Am. Chem. Soc.* **2002**, *124*, 14558−14570.
(18) Schmelzer, K. R.; Kubala, L.; Newman, J. W.; Kim, I. H.; Eiserich, J. P.; Hammock, B. D. *Proc. Natl. Acad. Sci. U.S.A.* **2005**, *102*, 9772−9777.
(19) Moghaddam, M. F.; Grant, D. F.; Cheek, J. M.; Greene, J. F.; Williamson, K. C.; Hammock, B. D. *Nat. Med.* **1997**, *3*, 562−566.
(20) Node, K.; Huo, Y. Q.; Ruan, X. L.; Yang, B. C.; Spiecker, M.; Ley, K.; Zeldin, D. C.; Liao, J. K. *Science* **1999**, *285*, 1276−1279.
(21) Cronin, A.; Mowbray, S.; Durk, H.; Homburg, S.; Fleming, I.; Fisslthaler, B.; Oesch, F.; Arand, M. *Proc. Natl. Acad. Sci. U.S.A.* **2003**, *100*, 1552−1557.
(22) Newman, J. W.; Morisseau, C.; Harris, T. R.; Hammock, B. D. *Proc. Natl. Acad. Sci. U.S.A.* **2003**, *100*, 1558−1563.

10.1021/ja066150c CCC: $37.00

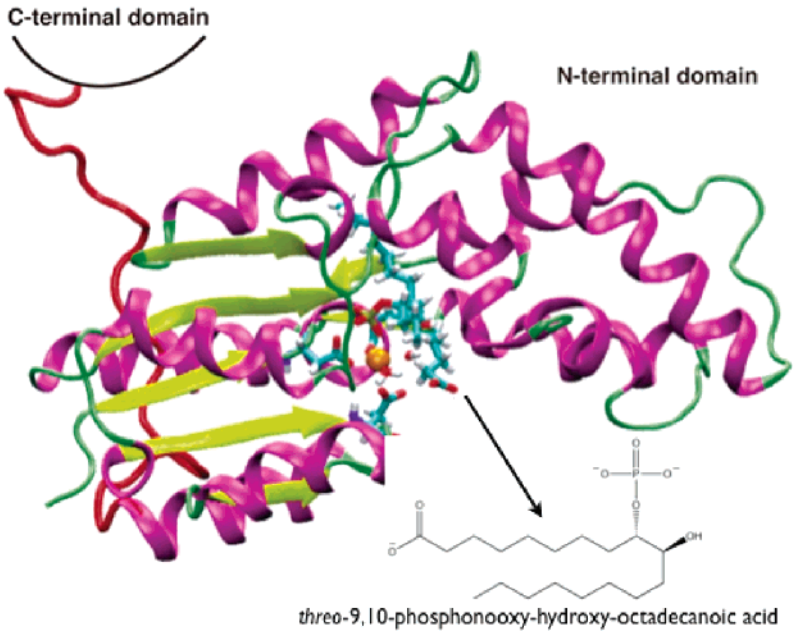

Figure 1. Cartoon of the sEH N-terminal domain fold. Secondary structures are colored in yellow (B-sheets), violet (α-helixes), and green (loops); the linker is colored in red. The orange sphere indicates the Mg^{2+} cofactor present in the active site, while coordinating ligands and the substrate molecule are depicted in stick representation and colored based on atom type.

N-terminal domain.[23] The structures of murine[24] and human[23] sEH enzymes reveal that the N-terminal domain adopts an α/β fold homologous to that of the haloacid dehalogenase (HAD) superfamily, the majority of which is composed of phosphotransferases. Structural comparison of the sEH phosphatase domain with several other proteins of the HAD superfamily reveals numerous conserved active-site residues[21,23−27] including a highly conserved nucleophilic aspartate residue (Asp9) and other residues (Asp11, Asp184, Asp185, Thr123, and Lys160) that surround the Mg^{2+} cofactor. The metal ion forms the center of a highly solvent exposed catalytic site situated in a ∼14 Å long hydrophobic tunnel suitable to accommodate an aliphatic substrate. It has been suggested that a gene fusion event caused the linkage of functionally associated proteins, leading to the formation of the two-domain/bifunctional structure of the sEH protein.[24,28,29]

On the basis of these findings, a two-step reaction scheme has been proposed that describes the double phosphoryl transfer taking place in the sEH phosphatase:[23] Step 1 is the nucleophilic attack on the phosphate group of the phosphoester substrate by Asp9, and protonation of the leaving group by either an intervening water molecule or Asp11; Step 2 is the hydrolysis of the phosphoenzyme intermediate via a nucleophilic attack at the scissile phosphorus atom by a water molecule (Scheme 1).

Interestingly, biochemical experiments showing that phosphorylated lipids are optimal substrates for the N-terminal phosphatase activity[22] suggest an in vivo circuit where phosphorylated diol products resulting from catalysis in the C-terminal domain are substrates for catalysis in the N-terminal activity.[16] Hence, the phosphatase activity of sEH may regulate its physiological function.[21,22] Since polyisoprenyl phosphate esters such as farnesyldiphosphate and geranylgeranyldiphos-

Scheme 1. Mechanism of Phosphatase Activity in sEH Proposed by Gomez et al.[23] and Investigated in Our Study[a]

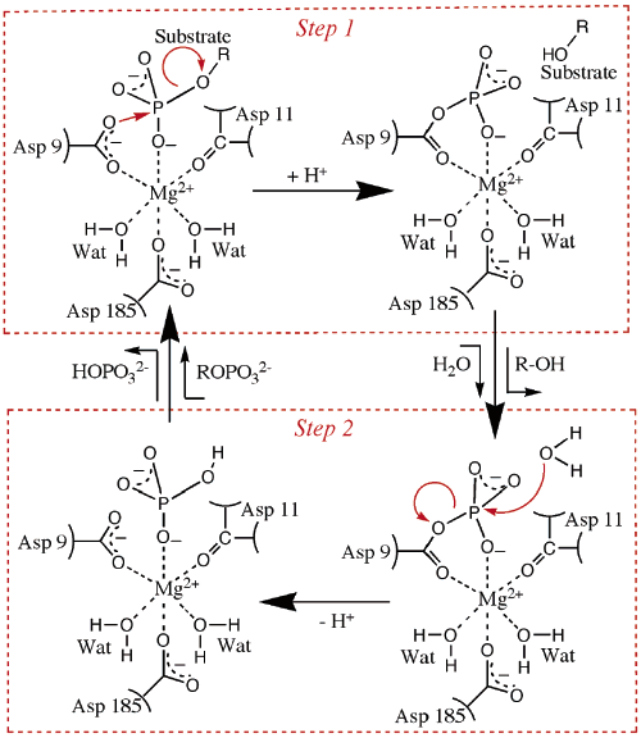

[a] Step 1: Phosphoenzyme intermediate formation via a nucleophilic attack at the phosphate group of the phosphoester substrate by Asp9. Step 2: Phosphoenzyme hydrolysis via a nucleophilic attack of a water molecule at the scissile phosphorus atom.

(23) Gomez, G. A.; Morisseau, C.; Hammock, B. D.; Christianson, D. W. *Biochemistry* **2004**, *43*, 4716−4723.
(24) Argiriadi, M. A.; Morisseau, C.; Hammock, B. D.; Christianson, D. W. *Proc. Natl. Acad. Sci. U.S.A.* **1999**, *96*, 10637−10642.
(25) Aravind, L.; Koonin, E. V. *Trends Biochem. Sci.* **1998**, *23*, 469−472.
(26) Koonin, E. V.; Tatusov, R. L. *J. Mol. Biol.* **1994**, *244*, 125−132.
(27) Morais, M. C.; Zhang, W. H.; Baker, A. S.; Zhang, G. F.; Dunaway-Mariano, D.; Allen, K. N. *Biochemistry* **2000**, *39*, 10385−10396.
(28) Enright, A. J.; Iliopoulos, I.; Kyrpides, N. C.; Ouzounis, C. A. *Nature* **1999**, *402*, 86−90.
(29) Marcotte, E. M.; Pellegrini, M.; Ng, H. L.; Rice, D. W.; Yeates, T. O.; Eisenberg, D. *Science* **1999**, *285*, 751−753.

phate are substrates for catalysis by the N-terminal domain, a possible physiological function in sterol synthesis or inflammation[30] is also suggested. Although further studies are needed to clarify its exact biological functions, it is possible that inhibitors of this activity may be useful in the treatment of inflammation, as recently demonstrated for inhibitors of the epoxide hydrolase activity of sEH.[18]

To follow up on our recent communication,[31] in which we reported preliminary mechanistic details of Step 1, here we describe the entire catalytic cycle with its free energy profile. In particular, we address previously ambiguous mechanistic aspects, such as the source of the proton that facilitates leaving group departure in Step 1, the activation of the nucleophilic water that dephosphorylates Asp9 during Step 2, the associative or dissociative character of the transition states for phosphoryl transfer, and the rate-determining chemical step in the catalytic cycle.

The chosen computational approach combines classical molecular dynamics (MD) and hybrid Car−Parrinello[32] (CP) quantum mechanical/molecular mechanics (QM/MM) methods. The MD simulations provide an extensive relaxation of the system and a sampling of the protein conformational space; the QM/MM[33−36] calculations allow the study of the phosphatase activity. Only the relevant active-site residues, the metal cation, and part of the substrate are treated at the quantum mechanical level, while the rest of the protein and the solvent waters are described at the classical MM level.

We provide first-principle-based interpretations of the experimental findings and propose a catalytic mechanism, which includes multievent reactions that proficiently facilitate water deprotonation and concerted proton transfers. The role of proton transfer in catalysis has been discussed extensively for several proteins such as carbonic anhydrase,[37−41] bacteriorhodopsin,[42] photosynthetic reaction center,[43,44] and others (see, for example, refs 45−47). It is accepted that the rate of localized proton transfers in the enzyme is principally modulated by electrostatic interactions in the active site.[33] On the other hand, long-range proton transfers in biological systems are still poorly understood at a quantitative level, while it is commonly proposed that they occur through hydrogen bond wires formed by water molecules or protein side chains.[48−50] Yet, it is still debated if the number of water molecules and their structural organization in a bridging hydrogen bond wire can favor a concerted or stepwise mechanism for proton transfers.[37,41,51] Here, we will use the term "proton shuttle" to distinguish the fast sequence of concerted proton transfers from stepwise proton transfers. We show that metal substrate connecting water bridges (WB) allow for efficient transfer of protons necessary for nucleophile formation and leaving group stabilization. These proton shuttles are concomitant with the enzymatic phosphoryl transfer reactions catalyzed by the sEH phosphatase. Finally, our findings can likely be generalized to the metal-dependent phosphatases belonging to the HAD superfamily.

Methods

Structural Model. Calculations are based on the crystallographic structure of Gomez et al. (PDB entry code 1VJ5, 2.35 Å resolution).[23] This structure contains the sEH protein (555 residues) with Mg^{2+}−HPO_4^{2-} in the N-terminal domain, and the inhibitor *N*-cyclohexyl-*N*′-(4-iodophenyl)urea in the C-terminal domain. Due to the system size and supported by experiments showing no correlation between the different catalytic activities in the two domains,[21] we considered in our study only the N-terminal domain (229 residues), including the *threo*-9-10-phosphonooxyhydroxyoctadecanoic acid substrate molecule.[52] This enzyme/substrate model is based on the binding mode proposed by Gomez et al.[23]

MD Simulations. Molecular dynamics is used to equilibrate the solvated enzyme/substrate complex (∼31 000 atoms) and provide a suitable model of the Michaelis complex for subsequent CP QM/MM calculations.[53] The AMBER force field[54] is adopted for the simulations, while the NAMD package[55] is used for the MD engine. A ∼10-ns simulation of MD is collected. The setup procedure and RMSD data are reported in the Supporting Information.

QM/MM MD Simulations. The reaction paths are investigated using CP QM/MM simulations, where the reactive part of the complex, namely the Mg^{2+} cation and its six ligands Asp9, Asp185, the backbone carbonyl of Asp11 (side chain not included due to its remote position from the reactive region), two/three water molecules, and the phosphate group of the substrate molecule (Figure 2, QM atoms highlighted), is treated at the quantum mechanical level (DFT-BLYP)[56,57] and the remaining part at the classical mechanics level (AMBER force field). This approach has been shown to accurately describe a wide variety of enzymatic systems,[58] in particular metalloenzymes[31,59] and DNA complexes.[60] CP calculations have also been used to correctly predict relative pK_a values.[61−63] The valence electrons are described by a basis set superposition error-free plane wave expansion up to a cutoff of 70 Ry. A 15 × 15 × 15 Å^3 supercell is used for the QM part of the system.

(30) Tran, K. L.; Aronov, P. A.; Tanaka, H.; Newman, J. W.; Hammock, B. D.; Morisseau, C. *Biochemistry* **2005**, *44*, 12179−12187.
(31) De Vivo, M.; Ensing, B.; Klein, M. L. *J. Am. Chem. Soc.* **2005**, *127*, 11226−11227.
(32) Car, R.; Parrinello, M. *Phys. Rev. Lett.* **1985**, *55*, 2471−2474.
(33) Warshel, A. *Annu. Rev. Biophys. Biomol. Struct.* **2003**, *32*, 425−443.
(34) Warshel, A.; Levitt, M. *J. Mol. Biol.* **1976**, *103*, 227−249.
(35) Field, M. J.; Bash, P. A.; Karplus, M. *J. Comput. Chem.* **1990**, *11*, 700−733.
(36) Gao, J. L.; Truhlar, D. G. *Annu. Rev. Phys. Chem.* **2002**, *53*, 467−505.
(37) Braun-Sand, S.; Strajbl, M.; Warshel, A. *Biophys. J.* **2004**, *87*, 2221−2239.
(38) Schutz, C. N.; Warshel, A. *J. Phys. Chem. B* **2004**, *108*, 2066−2075.
(39) Lu, D. S.; Voth, G. A. *J. Am. Chem. Soc.* **1998**, *120*, 4006−4014.
(40) Isaev, A.; Scheiner, S. *J. Phys. Chem. B* **2001**, *105*, 6420−6426.
(41) Cui, Q.; Karplus, M. *J. Phys. Chem. B* **2003**, *107*, 1071−1078.
(42) Wikstrom, M. *Curr. Opin. Struct. Biol.* **1998**, *8*, 480−488.
(43) Sham, Y. Y.; Muegge, I.; Warshel, A. *Proteins: Struct., Funct., Genet.* **1999**, *36*, 484−500.
(44) Lancaster, C. R. D.; Michel, H.; Honig, B.; Gunner, M. R. *Biophys. J.* **1996**, *70*, 2469−2492.
(45) Hofacker, I.; Schulten, K. *Proteins: Struct., Funct., Genet.* **1998**, *30*, 100−107.
(46) Florian, J.; Goodman, M. F.; Warshel, A. *J. Am. Chem. Soc.* **2003**, *125*, 8163−8177.
(47) Burykin, A.; Warshel, A. *Biophys. J.* **2003**, *85*, 3696−3706.
(48) Nagle, J. F.; Morowitz, H. J. *Proc. Natl. Acad. Sci. U.S.A.* **1978**, *75*, 298−302.
(49) Nagle, J. F.; Mille, M. *J. Chem. Phys.* **1981**, *74*, 1367−1372.
(50) Agmon, N. *Chem. Phys. Lett.* **1995**, *244*, 456−462.
(51) Konig, P. H.; Ghosh, N.; Hoffmann, M.; Elstner, M.; Tajkhorshid, E.; Frauenheim, T.; Cui, Q. *J. Phys. Chem. A* **2006**, *110*, 548−563.
(52) Incorrectly called *erythro* in ref 31.
(53) Laio, A.; VandeVondele, J.; Rothlisberger, U. *J. Chem. Phys.* **2002**, *116*, 6941−6947.
(54) Cornell, W. D.; Cieplak, P.; Bayly, C. I.; Gould, I. R.; Merz, K. M.; Ferguson, D. M.; Spellmeyer, D. C.; Fox, T.; Caldwell, J. W.; Kollman, P. A. *J. Am. Chem. Soc.* **1995**, *117*, 5179−5197.
(55) Kale, L.; Skeel, R.; Bhandarkar, M.; Brunner, R.; Gursoy, A.; Krawetz, N.; Phillips, J.; Shinozaki, A.; Varadarajan, K.; Schulten, K. *J. Comput. Phys.* **1999**, *151*, 283−312.
(56) Becke, A. D. *Phys. Rev. A* **1988**, *38*, 3098−3100.
(57) Lee, C. T.; Yang, W. T.; Parr, R. G. *Phys. Rev. B* **1988**, *37*, 785−789.
(58) Carloni, P.; Rothlisberger, U.; Parrinello, M. *Acc. Chem. Res.* **2002**, *35*, 455−464.
(59) Dal Peraro, M.; Llarrull, L. I.; Rothlisberger, U.; Vila, A. J.; Carloni, P. *J. Am. Chem. Soc.* **2004**, *126*, 12661−12668.
(60) Magistrato, A.; Ruggerone, P.; Spiegel, K.; Carloni, P.; Reedijk, J. *J. Phys. Chem. B* **2006**, *110*, 3604−3613.
(61) Davies, J. E.; Doltsinis, N. L.; Kirby, A. J.; Roussev, C. D.; Sprik, M. *J. Am. Chem. Soc.* **2002**, *124*, 6594−6599.
(62) Ivanov, I.; Klein, M. L. *J. Am. Chem. Soc.* **2002**, *124*, 13380−13381.
(63) Ivanov, I.; Chen, B.; Raugei, S.; Klein, M. L. *J. Phys. Chem. B* **2006**, *110*, 6365−6371.

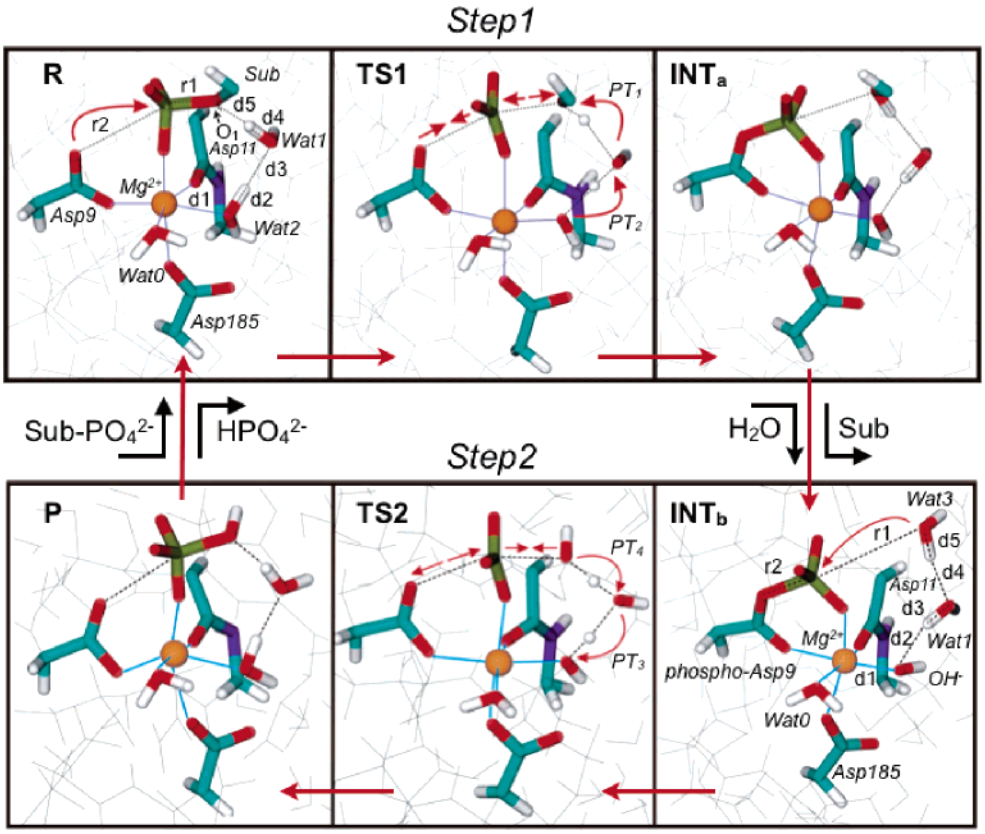

Figure 2. Selected snapshots taken from our computer simulations of the two investigated phosphoryl transfers comprising the catalytic cycle. (Top) Nucleophilic attack of Asp9 at the Mg^{2+}-coordinated phosphoryl group, with substrate cleavage and phosphoenzyme intermediate formation **INTa**. In the middle, the transition state structure **TS1** shows the concomitant proton shuttle (labeled PT1 and PT2) from a Mg^{2+}-coordinated water molecule to the leaving group oxygen via a bridging solvent water. (Bottom) Second phosphoryl transfer from the phospho-Asp9 to one attacking solvent water, leading to the product state, with now a second proton shuttle (labeled PT3 and PT4 in **TS2**) traveling in the reverse direction to create the nucleophile OH^-.

The interactions between valence electrons and ionic cores are described with norm-conserving Martins−Troullier pseudopotentials.[64] Car−Parrinello molecular dynamics simulations are carried out with a time step of 0.12 fs (totally ∼100 ps) and a fictitious electron mass of 900 au; constant temperature simulations are achieved by coupling the system with a Nosé−Hoover[65,66] thermostat at 500 cm^{-1} frequency. The interactions between the MM and QM regions are treated as in ref 53. Also, a rigorous treatment of the electrostatic interaction between QM and MM regions is implemented as in ref 67.

The protocol of the QM/MM calculations includes an initial equilibration of the MD starting snapshot: first, we performed a short simulation where only the MM part is free to move for ∼500 steps, while the QM part is kept frozen. Then, the whole system is allowed to move and heat up to 300 K (∼2 ps of free QM/MM dynamics). A configuration from the equilibrated simulations is used to initiate the constrained QM/MM calculations. The phosphate transfer reactions are described with a reaction coordinate (RC) defined as the difference between the length of the forming bond and that of the breaking bond. So-called blue-moon ensemble simulations are carried out of this system constrained at different values of the reaction coordinate, leaving all other degrees of freedom free to evolve. The catalytic reaction pathways are characterized in terms of (i) free energy profiles calculated using thermodynamic integration,[68] (ii) variation of critical bond lengths, averaged over the last ∼1.5 ps of each constrained CP QM/MM simulation, and (iii) variation of molecular charges along the reaction paths calculated by the "atoms in molecules" partitioning scheme.[69] Charges are averaged over 20 statistically independent snapshots extracted for every point along the reaction coordinate from the constrained simulations. We stress that the estimation of the present free energy, which employs input from costly ab initio calculations, should be considered approximate. For a more accurate estimation of the enzymatic activation free energies, several independent paths should be considered,[70] which unfortunately is currently beyond the available computational resources.

Results and Discussion

Step 1: Phosphoenzyme Formation. The free energy surface (FES) of the first step of the enzymatic reaction was computed using constraint dynamics, as explained in the Methods section. Constrained CP QM/MM simulations of 3−4 ps were performed for 14 points of different RC values, ranging from −1.95 to +1.95 Å. The RC was taken to be the difference between the length of breaking and forming bonds (RC = *r1* − *r2*; Figure 2, label in **R**). This RC is the minimal and natural choice describing the chemical reaction,[71,72] while all other degrees of freedom are left free.

The shape of the resulting FES (Figure 3) is characterized by two minima−the reactant state (**R**) constituting the Michaelis−Menten complex and the phosphoenzyme intermediate state

(64) Troullier, N.; Martins, J. L. *Phys. Rev. B* **1991**, *43*, 8861−8869.
(65) Nosé, S. *J. Chem. Phys.* **1984**, *81*, 511−519.
(66) Hoover, W. G. *Phys. Rev. A* **1985**, *31*, 1695−1697.
(67) Laio, A.; VandeVondele, J.; Rothlisberger, U. *J. Phys. Chem. B* **2002**, *106*, 7300−7307.
(68) Ciccotti, G.; Ferrario, M.; Hynes, J. T.; Kapral, R. *Chem. Phys.* **1989**, *129*, 241−251.
(69) Bader, R. F. W. *Atoms in Molecule: A Quantum Theory*; Oxford University Press: Oxford, 1990.
(70) Klahn, M.; Braun-Sand, S.; Rosta, E.; Warshel, A. *J. Phys. Chem. B* **2005**, *109*, 15645−15650.
(71) Akola, J.; Jones, R. O. *J. Phys. Chem. B* **2003**, *107*, 11774−11783.
(72) Meijer, E. J.; Sprik, M. *J. Am. Chem. Soc.* **1998**, *120*, 6345−6355.

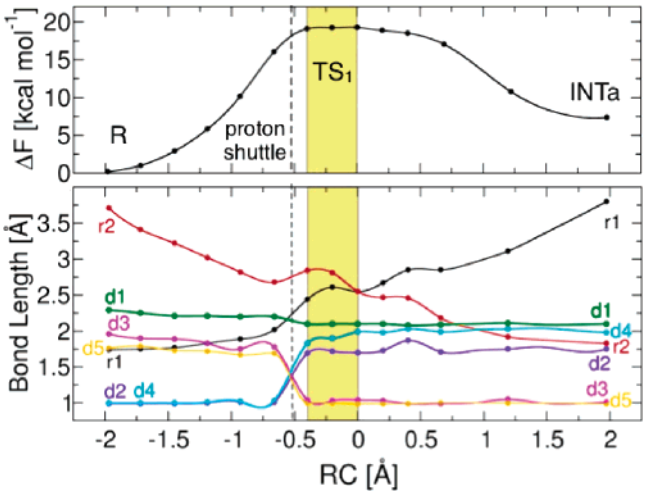

Figure 3. Free energy profile (top) and selected average bond distances (bottom) along the first catalytic step of phosphoenzyme formation (**INTa**). Bond distance labels as in Figure 2; notably, *r1* and *r2* are the breaking and forming P−O bond lengths, respectively. The proton shuttle occurs at RC ≈ −0.5A (vertical dashed line), just before the system reaches the TS plateau (orange region). Note the shortening of the Mg^{2+}−ligand distance, d1, upon proton donation and transfer along the H-bond wire (d2/d3 and d4/d5 crossing).

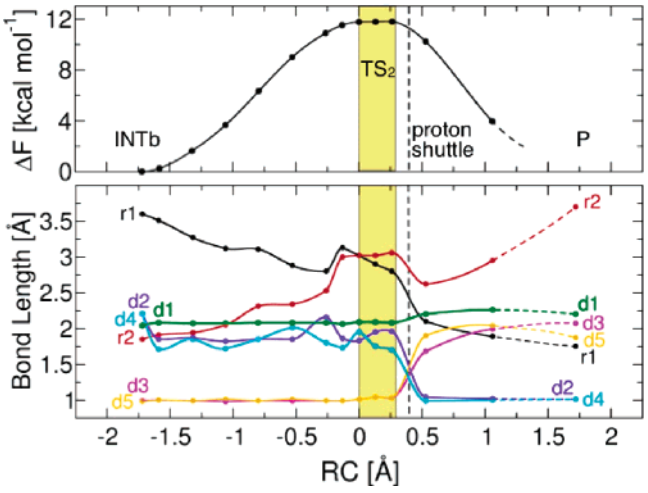

Figure 4. Free energy profile (top) and selected average bond distances (bottom) along the second catalytic step. Bond distance labels as in Figure 2 (**INTb** panel). Here, the proton shuttle (dashed vertical line) occurs in the reverse direction (note the d2/d3 and d4/d5 crossing) after the TS plateau (orange region).

(**INTa**) including the phosphorylated Asp9 − separated by a single TS maximum (**TS1**). Simulations of the initial reactant state **R** (RC = −1.95 Å) shows a well-structured H-bond network that stabilizes the Mg^{2+}-centered catalytic site. It includes a hydrogen bond wire formed by water molecule WAT1, which is bridging the Mg^{2+}-bound water WAT2 and the oxygen O_1 of the substrate leaving group (Mg^{2+}···WAT2···WAT1···O_1). The spontaneous insertion of WAT1 between WAT2 and O_1 was observed during both unconstrained CP QM/MM dynamics[31] and classical MD, facilitated by the high solvent exposure of the catalytic site region.

Upon increasing the RC from **R** (RC = −1.95 Å) to **TS1** (RC = −0.6 Å), the forming bond *r2* shortens from ∼3.75 to ∼2.65 Å. The length of the bond being broken, *r1*, increases simultaneously to ∼2.05 Å (as shown in Figure 3).

At RC ≈ −0.5 Å (average value validated after a reverse procedure along the same RC), a spontaneous key event occurs: the advanced cleavage of *r1* (∼2.21 Å) produces a rise in the basicity of O_1, which initiates a proton shuttle involving a double proton transfer along the H-bond wire formed by WAT2−WAT1−O_1 (see **TS1** in Figure 2). (i) First, O_1 receives a proton from WAT1, forming a good leaving group (SUB−O_1H) by saturating the negative charge on O_1 (PT1 in Figure 2). (ii) Immediately after, the incipient hydroxide ion, now bridging SUB−O_1H and WAT2, accepts a proton from WAT2 (PT2 in Figure 2). This second proton transfer forms again a bridging water molecule (WAT1) while transforming WAT2 into a hydroxide ion stabilized by Mg^{2+} coordination. The stronger metal−ligand electrostatic interaction is evidenced by distance d1 (Figure 3), which decreases from its initial average of ∼2.25 to ∼2.05 Å after the WB-mediated proton shuttle. At RC = −0.4 Å, *r1* rapidly elongates leading to its definitive cleavage, and a narrow interval (−0.4 ≤ RC ≤ 0 Å, orange area in Figure 3) is reached in which the average constraint force is essentially equal to zero, indicating a flat TS region. Initially, the breaking of *r1* causes a moderate increase in *r2* as well, then followed by values where progressively *r1* and *r2* reach the same length at RC = 0 Å (*r1* = *r2* ≈ 2.56 Å). Hence, the phosphoryl transfer reaction shows a metaphosphate-like species in the TS region.

At RC = 0.2 Å, the average constraint force changes signs, indicating that the system is falling into the first product well (i.e., phosphoenzyme intermediate **INTa**). Further sampling of the RC from ∼0.4 to ∼2.0 Å shows the formation of the **INTa** metastable state where the average constraint force is again equal to zero. At this local minimum of the FES, *r2* is equal to ∼1.83 Å, while *r1* has reached a value of ∼3.83 Å (Figure 3).

Step 2: Phosphoenzyme Hydrolysis. The second phosphoryl transfer reaction was simulated after removal of the unphosphorylated lipid substrate (SUB−O_1H) from the final state of the first step, assuming its departure after the phosphoenzyme formation, followed by water molecules filling the remaining cavity. First, the system is again equilibrated by classical MD, keeping the QM atoms fixed as in the **INTa** structure. After ∼300 ps, a snapshot has been selected to initiate the constrained CP QM/MM calculations. High similarity of the charge distribution in the catalytic site (further discussed hereafter) before and after substrate removal and re-equilibration indicates that these modifications can be expected to have only very minor effects. One additional water molecule (WAT3) was selected to be in the QM region for the second reaction step (Figure 2, **INTb**). The same type of RC (RC = *r2* − *r1*, Figure 2) and procedure as applied to the previous step are used to now investigate Step 2 (RC ranging from −1.75 to +1.75 Å).

The FES of the phosphoenzyme hydrolysis is characterized by the starting phospho-intermediate structure **INTb**, the transition state **TS2**, and the final product **P** (Figure 4). The **INTb** point (RC = −1.75 Å) includes the nucleophilic water WAT3, in a plausible orientation for attacking the scissile phosphorus atom. The H-bond network is stable, as well as the Mg^{2+}-centered catalytic site, while a new metal substrate connecting hydrogen bond wire is formed: WAT1 is now bridging the Mg^{2+}-bound OH^- ion and WAT3.

Upon increasing the RC from −1.75 to −0.26 Å, the length *r1* of the bond to be formed progressively decreases, from ∼3.65 to ∼2.80 Å. The breaking bond is cleaved at RC = −0.80 Å,

where *r2* reaches ~2.30 Å, indicating a nominal stability of the phosphoenzyme intermediate,[73] which releases the PO_3^- group rather easily. The breaking P−O bond length *r2* continues to increase until RC = 0.0 Å, where it reaches a value of ~3.0 Å. Note the steep increase of *r2* at −0.52 ≤ RC ≤ −0.26 Å, which causes a temporary increase of *r1* as well; the latter, however, continues to decrease after this interval.

At 0.0 ≤ RC ≤ +0.26 Å (orange area in Figure 4), the average constraint force is essentially zero, indicating that the TS region is reached. Within this interval, *r2* maintains a value of ~3.0 Å, while *r1* decreases to ~2.8 Å at RC = +0.26 Å. At RC ≈ +0.4 Å (average value validated after reverse procedure along the same RC), a second proton shuttle occurs in the reverse direction with respect to the proton shuttle observed in Step 1; that is, a late deprotonation of the nucleophile WAT3 is facilitated by the proton acceptor represented by the hydroxide ion bound to Mg^{2+}. First, the OH^- receives a proton from the bridging WAT1 (PT3 in Figure 2); immediately after, the incipient OH^- ion, now bridging WAT2 and WAT3, receives a proton from WAT3 (PT4 in Figure 2). The increased nucleophilicity of WAT3, transformed into OH^-, facilitates its attack at the scissile phosphorus atom, as shown in Figure 4 by the sharp decrease of *r1* (and even of *r2* due to its coupling to *r1* via the constrained RC). The initial, Mg^{2+}-coordinated, OH^- ligand is transformed into WAT2, causing an increase in distance d1 from its initial average value of ~2.05 to ~2.25 Å.

At RC = +0.52 Å, the average constraint force changes signs, indicating that the system has crossed the TS and can evolve downhill toward the product state. At RC = +1.10 Å, the product state is reached in which the $HO-PO_3^{2-}$ group is formed. Upon removal of the constraint, the system falls further into the product well, taking a final value of RC ≈ +1.75 Å with *r1* ≈ 1.75 Å and *r2* ≈ 3.70 Å.

We emphasize that each proton shuttle herein described occurs spontaneously and completely (i.e., without stepwise intermediate states). Although we cannot definitely rule out a possible stepwise mechanism for the observed sequences of proton transfers (PT1, PT2, PT3, and PT4), our calculations indicate the concerted mechanism as a favorable one for proton transfers in sEH phosphatase, at least for this level of theory.

Charge Distribution along the Reactions. Both reaction paths can be monitored by charge variations of relevant molecular moieties, as reported in Figure 5. At the initial state **R**, charge-transfer effects play a role at the metal center: Mg^{2+} cation ($q = -1.77$) has accepted electron density from the Asp ligands and $SUB-O_1-PO_3^{2-}$ group ($q = -1.75$). Starting from RC ≈ −0.8 Å, a considerable amount of charge is transferred along the breaking P−O bond *r1*; the scissile PO_3^- group gains electron density from the leaving substrate (~−0.65 → ~−1.00), evidencing the formation of the metaphosphate-like transition state. This local charge redistribution at the leaving group primes the first proton shuttle event at RC ≈ −0.5: $SUB-O_1$ receives a proton from WAT1 (PT1), followed by the transformation of WAT2 in a hydroxide ion (PT2) stabilized by the favorable electrostatic interaction with Mg^{2+}. At **TS1,** the PO_3^- as well as the other moieties conserve their molecular charge until **INTa** formation at RC ≈ 2.0 Å, where the transfer of charge from the PO_3^- to Asp9 accompanies and promotes the formation of the new bond *r2*.

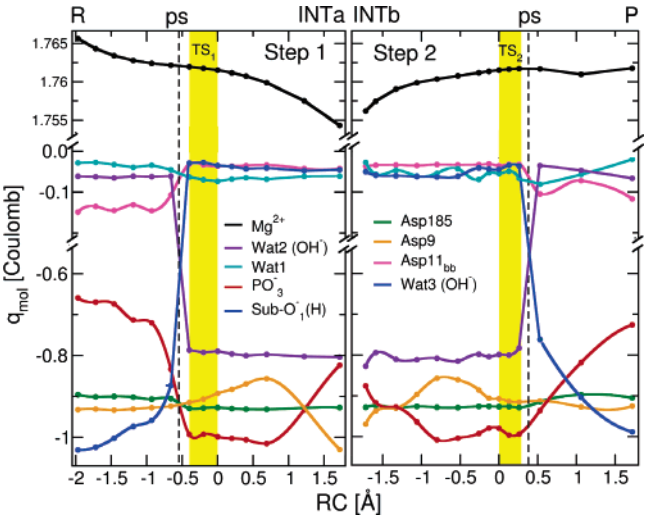

Figure 5. Average charges of selected molecular moieties in the active site along the first (left panel) and second (right panel) phosphoryl transfer reaction (see color coding in figure). The metaphosphate-like transition state formation along both transfers is shown by the temporary increase of negative charge of the PO_3^- group (red line) along the reaction. The crossing of blue and violet lines shows the charge transfer along the H-bond wire during the proton shuttles (dashed vertical lines).

In Step 2, at the initial **INTb** state, the charge distribution is virtually equal to that of the final **INTa** of Step 1. Thus, the substitution of the substrate by water molecules does not perturb the system. Upon reaching **TS2**, significant changes in the charge distribution accompany the second phosphoryl transfer: the PO_3^- group shows the formation of a metaphosphate-like transition state through a gain of negative charge (~−0.90 → ~−1.10), partially counterbalanced by the charge increase of Asp9 (~−0.95 → ~−0.85). Just after **TS2**, a relevant charge-transfer interaction between PO_3^- and the approaching WAT3 primes the second proton shuttle (PT3−PT4) characterized by the final formation of the Mg^{2+}-bound WAT2. Finally, the system reaches the products state in which the electronic charge distribution recovers values similar to that in **R**.

It is interesting to notice the nearly perfect mirror symmetry of the redistribution of electronic charge along the two steps of the reaction (Figure 5). For instance, the Mg^{2+} charge shows a progressive decrease along Step 1 and a mirrorlike trend during Step 2. The charge symmetry drives the reaction to a symmetrical dynamics of the catalytic cycle: the proton shuttle events occur just before **TS1** and just after **TS2**, respectively, along Steps 1 and 2. The charge-transfer effects taking place along the breaking−forming bonds *r1* and *r2* seem to play the major role in promoting the proton shuttles.

Energetic of the Enzymatic Reactions. The free energy profiles of the two phosphoryl transfer reactions were computed by integration of the average forces of constraint as described in the Methods section and plotted in Figure 3 for Step 1 and in Figure 4 for Step 2. The free energy barrier determined for the first pathway **R** → **TS1** → **INTa** is ~19 ± 0.5 kcal mol^{-1}. Although there is some uncertainty related to the calculated free energy, it is interesting to note that this value agrees well with the experimental number related to the whole catalytic activity, which is ~18 kcal mol^{-1} calculated according to the enzymatic reaction theory using the $k_{cat} = 0.35\ s^{-1}$ reported for the substrate used in our study.[22] Formation of **INTa** is endothermic by 10 kcal mol^{-1} with respect to the reactant complex **R**, with

(73) Barth, A.; Bezlyepkina, N. *J. Biol. Chem.* **2004**, *279*, 51888−51896.

a somewhat larger uncertainty of ~3 kcal mol^{-1} due to larger fluctuations in the force of constraint in the simulations of the last part of the first step. The free energy barrier of the second pathway **INTb** → **TS2** → **P** is ~12 ± 1.5 kcal mol^{-1}, which compares well with the value of ~10.7 kcal mol^{-1} obtained for the hydrolysis of acetylphosphate.[14] Although the relative barrier heights would indicate Step 1 as the rate-limiting chemical step, the free energies of **TS1** and **TS2** with respect to the reactant complex are more or less equal. However, a quantitative comparison is hindered by the unknown energy difference between **INTa** and **INTb** (from the replacement of the leaving substrate group by solvent water molecules in the catalytic site), which can be expected to shift the free energy profile of Step 2 with respect to that of Step 1 by a few kilocalories per mole. If we are allowed to assume that the two steps are sufficiently disconnected by the relatively slow diffusive process of substrate removal from the cavity after Step 1, **INTb** can be considered a new equilibrated reference state from which the system needs to be reactivated to reach **TS2** and undergo Step 2. As the second activation of ~12 kcal mol^{-1} is much smaller than the first activation of ~19 kcal mol^{-1}, the first step can be considered to be the rate-limiting chemical step of the overall process.

No pentavalent phosphorane intermediate such as that observed in β-phosphoglucomutase[74−78] was observed along Steps 1 and 2 in these computations, in agreement with previous computational studies of phosphoryl transfer in HIV-1 integrase and cyclin-dependent kinase 2.[79,80] Neither *r1* nor *r2* show values resembling a phosphorane species in the TS regions. Although such an intermediate cannot definitely be ruled out, due to the flat nature of those regions, it would significantly affect neither the reaction profile nor the reaction rate,[81] since its energy could only be slightly lower (~1−2 kcal mol^{-1}) of that of the surrounding TSs.

To appreciate the role of the WB-mediated proton shuttles in forming a better nucleophile and leaving group, we investigated alternative pathways that start from the same initial configurations used for studying Steps 1 and 2. Importantly, in these alternative pathways (referred to as Step 1b and Step 2b hereafter), the WB molecule is manually removed. We also apply a restraint on distance d1, so that both WAT2 (along Step 1b) and OH$^-$ (along Step 2b) maintain their coordination to the Mg^{2+} cation. Thus, we induce the system toward reaction paths in which the formation of a favorable hydrogen bond wire, such as that present along Steps 1 and 2, is impossible.

Along the alternative pathways, Step 1b shows a phosphoryl transfer mechanism similar to that found in Step 1. As expected, no proton shuttle is involved in the formation of a good leaving group. This mechanism has a free energy barrier of ~36 kcal mol^{-1}, which corresponds to a reaction rate that is ~12 orders of magnitude slower than the pathway including the proton shuttle. Also along Step 2b, the lack of a WB proton shuttle strongly discourages the reaction. Moreover, without the WB molecule WAT1, the catalytic site undergoes major structural rearrangements that lead to the loss of coordination around the metal ion. In other words, even though the system can reach the **TS2** region, in which WAT3 attacks the scissile phosphorus atom with a barrier of ~24 kcal mol^{-1} (~9 orders of magnitude slower than the WB-mediated pathway), the absent deprotonation of the nucleophile WAT3 prevents the formation of the final reaction product. To avoid the latter problem, we have alternatively simulated the direct attack of a hydroxide ion that could have been formed by early WAT3 deprotonation, assuming the formation of WAT2 in **INTb** (Supporting Information). However, if a free OH$^-$ ion is present in the catalytic site, we observed its immediate spontaneous protonation by WAT2, again forming our starting structure **INTb** in Step 2.

The enzymatic barrier can be compared to that of the phosphoryl transfer reaction in water, for which a wealth of literature is available.[71,81−88] For our case, the study of Akola and Jones[71] is the most relevant one since it concerns the hydrolysis of the Mg-complexed methyl thiphosphate in water, studied by means of CPMD calculations. The barriers found for different mechanisms (dissociative and associative) are ~35−40 kcal mol^{-1}, which compare well with barriers reported by Florian and Warshel[81] for methyl phosphate hydrolysis in water (~40 kcal mol^{-1}). Thus, these studies further show the efficiency of the enzymatic mechanism herein proposed.

In summary, within the limited/allowed size of our QM system and the necessarily restricted sampling, this study demonstrates the significance of metal substrate connected H-bond wires via WB molecules, which enable the efficient proton shuttle events involved in nucleophile and leaving group stabilization and that are concomitant with the phosphoryl transfer reactions catalyzed in sEH. The crucial catalytic role of the Mg^{2+} cation, essentially performed through its electrostatic and chelating effects and its ability to reduce pK_a of the first Mg^{2+} solvation shell by several units,[89] facilitates water deprotonation, giving origin to the proton shuttle events. Thus, as a general rule, we emphasize the significance to include explicit solvation waters in the QM calculations in studying phosphoryl transfers. In this regard, it is important to mention that the study of Florian and Warshel,[81] as well as recent reconsiderations of the reaction mechanism of phosphate hydrolysis by Klahn and coauthors,[70] could not observe such WB-mediated proton shuttles concomitant to phosphoryl transfers since these studies did not include solvation waters in the system.

Conclusions

In this article, we have presented a computational investigation of the novel phosphatase activity recently discovered in

(74) Lahiri, S. D.; Zhang, G. F.; Dunaway-Mariano, D.; Allen, K. N. *Science* **2003**, *299*, 2067−2071.
(75) Blackburn, G. M.; Williams, N. H.; Gamblin, S. J.; Smerdon, S. J. *Science* **2003**, *301*, 1184c.
(76) Allen, K. N.; Dunaway-Mariano, D. *Science* **2003**, *301*, 1184d.
(77) Tremblay, L. W.; Zhang, G. F.; Dai, J. Y.; Dunaway-Mariano, D.; Allen, K. N. *J. Am. Chem. Soc.* **2005**, *127*, 5298−5299.
(78) Holmes, R. R. *Acc. Chem. Res.* **2004**, *37*, 746−753.
(79) Bernardi, F.; Bottoni, A.; De Vivo, M.; Garavelli, M.; Keseru, G.; Naray-Szabo, G. *Chem. Phys. Lett.* **2002**, *362*, 1−7.
(80) Cavalli, A.; De Vivo, M.; Recanatini, M. *Chem. Commun.* **2003**, 1308−1309.
(81) Florian, J.; Warshel, A. *J. Phys. Chem. B* **1998**, *102*, 719−734.
(82) Bunton, C. A.; Llewellyn, D. R.; Oldham, K. G.; Vernon, C. A. *J. Chem. Soc.* **1958**, 3574−3587.
(83) Florian, J.; Warshel, A. *J. Am. Chem. Soc.* **1997**, *119*, 5473−5474.
(84) Florian, J.; Aqvist, J.; Warshel, A. *J. Am. Chem. Soc.* **1998**, *120*, 11524−11525.
(85) Aqvist, J.; Kolmodin, K.; Florian, J.; Warshel, A. *Chem. Biol.* **1999**, *6*, R71−R80.
(86) Hu, C. H.; Brinck, T. *J. Phys. Chem. A* **1999**, *103*, 5379−5386.
(87) Ma, B. Y.; Xie, Y. M.; Shen, M. Z.; Schleyer, P. V.; Schaefer, H. F. *J. Am. Chem. Soc.* **1993**, *115*, 11169−11179.
(88) Grigorenko, B. L.; Rogov, A. V.; Nemukhin, A. V. *J. Phys. Chem. B* **2006**, *110*, 4407−4412.
(89) Lightstone, F. C.; Schwegler, E.; Hood, R. Q.; Gygi, F.; Galli, G. *Chem. Phys. Lett.* **2001**, *343*, 549−555.

the N-terminal domain of the bifunctional sEH enzyme. Importantly, this domain includes conserved catalytic residues that participate in phosphatase activity in several other proteins of the HAD superfamily.[21,23−27] In particular, we have examined the two phosphoryl transfer reactions of phosphoenzyme formation (Step 1) and phosphoenzyme hydrolysis (Step 2) that make up the catalytic cycle of the phosphatase activity in sEH.

Both steps show an in-line nucleophilic substitution presenting a rather dissociative character, particularly pronounced in Step 2. No evidence of a phospharane species in the TS regions is found, but instead a planar metaphosphate-like transition state that well resembles crystal structures of TS analogues[90,91] is observed. The computed free energy barriers are in good agreement with experimental values, suggesting Step 1 (∼19 kcal mol^{-1}) as the rate-determining step of the catalytic cycle.

Chemical steps in phosphoryl transfer reactions are the protonation of the leaving group and the deprotonation of the attacking nucleophile. For sEH, however, the proton donor and acceptor in these steps were still unclear until now. In our simulations, we find that the role of the proton donor in Step 1 is performed by a water molecule acidified by coordination to Mg^{2+}. Because of its favorable position with respect to the leaving group of the substrate, which docks via the phosphoryl group to the same metal ion, the water ligand is connected to the leaving group via a short hydrogen bond wire involving a single bridging water molecule in the solvent-exposed cavity. A fast proton shuttle along this H-bond wire creates a favorable leaving group that departs concomitantly with P−O bond cleavage. In Step 2, the reverse process is observed, as now the Mg^{2+}-coordinated hydroxide ion accepts the proton from the attacking solvent molecule in a fast shuttle again via a single WB molecule. The facilitating proton shuttles are observed spontaneously and the phosphoryl transfer is reversible (showing a minimal hysteresis), indicating that the barrier for the proton transfer is very small. Quantum effects such as zero-point motion and tunneling, which were neglected in our calculations, would likely reduce such a barrier even further.

In conclusion, we have uncovered the efficient and elegant way in which the sEH enzyme performs a highly concerted multievent reaction sequence to accelerate phosphoryl transfer reactions. Overall, an important contribution in the enhancement of the catalytic efficiency comes from the nucleophile and leaving group stabilization via WB-mediated proton shuttles, mostly induced by the electrostatic effects of the metal ion. In fact, repression of these proton shuttles in our simulations leads to inhibition of the phosphatase activity. Due to the conservation of active-site residues in the N-terminal domain of sEH and other proteins of the HAD superfamily, we suggest a generalization of the mechanism presented herein to these metal-dependent phosphatases. Knowledge of TS geometries and charge distribution are also of practical interest, since it might eventually provide a blueprint for the design of specific transition state inhibitors.

Acknowledgment. We thank the NIH for financial support and the Pittsburgh Supercomputer Center (PSC) for computing time.

Supporting Information Available: Classical MD setup and data, RESP charges of catalytic residues implemented in the MD simulations, and snapshots illustrating the alternative pathways investigated (PDF, MPG). This material is available free of charge via the Internet at http://pubs.acs.org.

JA066150C

(90) Schlichting, I.; Reinstein, J. *Biochemistry* **1997**, *36*, 9290−9296.
(91) Schlichting, I.; Reinstein, J. *Nat. Struct. Biol.* **1999**, *6*, 721−723.